Disorder-driven glasslike thermal conductivity in colusite Cu_{26}V_{2}Sn_{6}S_{32} investigated by Mössbauer spectroscopy and inelastic neutron scattering

Christophe Candolfi, Gabin Guélou, Cédric Bourgès, Andrew R. Supka, Rabih Al Rahal Al Orabi, Marco Fornari, Bernard Malaman, Gérard Le Caër, Pierric Lemoine, Vincent Hardy, Jean-Marc Zanotti, Raju Chetty, Michihiro Ohta, Koichiro Suekuni, and Emmanuel Guilmeau

Phys. Rev. Materials **4**, 025404 — Published 19 February 2020

DOI: 10.1103/PhysRevMaterials.4.025404

Disorder-driven glass-like thermal conductivity in colusite $Cu_{26}V_2Sn_6S_{32}$ investigated by Mössbauer spectroscopy and inelastic neutron scattering

Christophe Candolfi,[1,*] Gabin Guélou,[2] Cédric Bourgès,[2] A. R. Supka,[3] Rabih Al Rahal Al Orabi,[3,4] M. Fornari,[3] Bernard Malaman,[1] Gérard Le Caër,[5] Pierric Lemoine,[6] Vincent Hardy,[2] Jean-Marc Zanotti,[7] Raju Chetty,[8] Michihiro Ohta,[8] Koichiro Suekuni,[9] Emmanuel Guilmeau[2,*]

[1] *Institut Jean Lamour, UMR 7198 CNRS – Université de Lorraine, 2 allée André Guinier-Campus ARTEM, BP 50840, 54011 Nancy Cedex, France*

[2] *Laboratoire CRISMAT, UMR 6508, CNRS, ENSICAEN, 6 Boulevard du Maréchal Juin, 14050 Caen Cedex 04, France*

[3] *Department of Physics and Science of Advanced Materials Program, Central Michigan University, Mt. Pleasant, Michigan 48859, United States*

[4] *Solvay, Design and Development of Functional Materials Department, AXEL' ONE Collaborative Platform − Innovative Materials, 87 Rue des Freres Perret − BP62, 69192 Saint Fons Cedex, France*

[5] *Institut de Physique de Rennes, UMR UR1-CNRS 6251, Université de Rennes I, Campus de Beaulieu, 35042 Rennes Cedex, France*

[6] *Université de Rennes, CNRS, ISCR – UMR 6226, F-35000 Rennes, France*

[7] *Laboratoire Léon Brillouin, CNRS-CEA (UMR 12), CNRS, Université Paris-Saclay, CEA Saclay, 91191 Gif-sur-Yvette Cedex, France*

[8] *Research Institute for Energy Conservation, National Institute of Advanced Industrial Science and Technology (AIST), Tsukuba, Ibaraki 305-8568, Japan*

[9] *Department of Applied Science for Electronics and Materials, Interdisciplinary Graduate School of Engineering Sciences, Kyushu University, Kasuga, Fukuoka 816-8580, Japan*

*Contact authors: emmanuel.guilmeau@ensicaen.fr; christophe.candolfi@univ-lorraine.fr

Abstract

The influence of structural disorder on the thermal transport in the colusite $Cu_{26}V_2Sn_6S_{32}$ has been investigated by means of low-temperature thermal conductivity and specific heat measurements (2 – 300 K), ^{119}Sn Mössbauer spectroscopy and temperature-dependent powder inelastic neutron scattering (INS). Variations in the high-temperature synthesis conditions act as a key parameter for tuning the degree of disorder in colusite compounds. Intriguingly, we find that even samples previously thought to be fully ordered are in fact weakly disordered. Mössbauer data clearly evidence that Sn atoms do not solely occupy the 6*c* site of the crystal lattice but are present on possibly both the Cu and V sites, leading to a random distribution of these three cations within the unit cell. Increasing the disorder in these materials tends to lead to a smearing out of the main features in the phonon density of states measured by INS. Although the evolution of the inelastic signal upon warming is well described by a quasi-harmonic approximation, elastic properties calculations indicate large average Grüneisen parameters, consistent with those determined experimentally from thermodynamic data. Intriguingly, increasing the level of disorder results in a decreased average Grüneisen parameter suggesting that the lowered lattice thermal conductivity is not driven by enhanced anharmonicity. These results provide experimental evidence to support that the remarkable changeover in the lattice thermal conductivity from crystalline to glass-like is solely driven by enhanced disorder accompanied by local lattice distortions.

I. Introduction

The structural disorder observed in various complex materials have important implications on the heat propagation. Introducing additional disorder through substitutions, formation of solid solutions or nanostructuration provides a simple, yet powerful strategy to lower the phonon transport and thus, to design well-crystallized materials with very low lattice thermal conductivity κ_L for thermal barrier coatings or thermoelectric applications.[1-3] The mass fluctuations and local distortions induced by some of these approaches act as scattering centers for acoustic phonons. In addition to enhanced point-defect scattering, interstitial atoms can also have a dramatic influence on κ_L. One prominent example is provided by the fluoride compound BaF_2 in which the substitution La for Ba requires a concomitant increase in the F content in order to preserve charge balance.[4,5] The short range order and strong local distortions induced by these additional F atoms on interstitial sites result in a transition from crystalline-like to glass-like thermal transport with κ_L values decreasing by nearly two orders of magnitude at 300 K.[4,5]

Colusites, a class of sulfur-based minerals, are another example of compounds where disorder can be used to control their electronic and thermal transport properties.[6-16] Remarkably, increasing the temperature at which the powders are consolidated results in dramatic changes in κ_L that undergoes a nearly fourfold decrease from 1.4 to 0.4 W m^{-1} K^{-1} at 300 K.[13] These lower κ_L values are the key characteristic that yields a spectacular improvement of their thermoelectric performances at high temperatures.[13] The modification in the thermal transport is believed to be tied to a concomitant increase in the unit cell disorder due to a mixed distribution of the Cu, V and Sn atoms, possibly accompanied by Cu interstitials.[13] The presence of these antisite defects are supported by defect formation energy calculations indicating that Cu/Sn and V/Sn antisite defects are the most probable.[13]

Experimentally, the random distribution of these aforementioned atoms has been evidenced by transmission electron microcopy experiments.[10] However, the exact role of this enhanced chemical disorder on the microscopic mechanisms governing κ_L is yet to be fully understood.

Here, we explore in more detail the nature and the influence of this inherent disorder on the lattice dynamics of colusites $Cu_{26}V_2Sn_6S_{32}$ prepared following two distinct synthesis routes, by means of ^{119}Sn Mössbauer spectroscopy, temperature-dependent powder inelastic neutron scattering (INS), low-temperature specific heat (C_p) and thermal conductivity (κ) measurements (2 – 300 K). Mössbauer spectroscopy, used as a sensitive probe of the chemical environment of the Sn atoms, evidences that both samples show some degree of disorder, even in the sample previously thought of as being perfectly ordered. Varying the high-temperature conditions of the consolidation process acts as an external parameter that tunes the degree of disorder which ultimately determines the character of the thermal transport. The temperature variations of the generalized vibrational density of states (GVDOS) is well captured by a quasi-harmonic model, further indicating that the significant decrease in κ_L is not driven by enhanced anharmonicity. These findings rather suggest that the higher degree of disorder achieved in some samples, and related to a mixed distribution of Cu, V and Sn atoms on several sites of the crystal structure accompanied by local lattice distortions, act as an efficient source of phonon diffusion.

II. Experimental methods

A. Sample preparation, structural and chemical characterizations

The two polycrystalline samples of chemical composition $Cu_{26}V_2Sn_6S_{32}$ were prepared by ball milling following the synthetic route described in detail in a prior study.[13] The phase-

purity of the ball-milled powders were subsequently checked by powder X-ray diffraction (PXRD). The PXRD patterns were found to be consistent with the $P\bar{4}3n$ space group of colusites.[6,7] The powders were consolidated using two distinct sets of temperature and pressure conditions. The first ingot was consolidated by spark plasma sintering at 873 K during 45 min. under a uniaxial pressure of 64 MPa with heating and cooling rates of 50 K min^{-1}. The second ingot was obtained by hot pressing at 1023 K for 1 h under a uniaxial pressure of 70 MPa with heating and cooling rates of 10 and 20 K min^{-1}, respectively. Hereafter, these two samples will be labeled as L and H, as in the prior study,[13] which refers to the low and high sintering temperatures used.

PXRD measurements were performed on the two obtained samples by grinding small pieces into fine powders. The data were collected at 300 K using a D8 Advance diffractometer (CuKα radiation with Ge(111) monochromator). The lattice parameter a of both samples, inferred from Rietveld refinements against the PXRD data, are consistent with those determined in Ref. 13 (Figure 1).

Bar-shaped samples for transport property measurements were cut from the consolidated pellets with a diamond-wire saw. Thermal conductivity κ was measured in the temperature range 2 – 300 K using the thermal transport option of a physical property measurement system (PPMS, Quantum Design). Electrical and thermal contacts on samples were realized by attaching copper bars with a small amount of conducting silver epoxy. Specific heat measurements were carried out in the same temperature range on small bulk pieces (~ 20 mg) using a relaxation method implemented on the He4 specific heat option of the PPMS. The lattice contribution to the thermal conductivity κ_L has been obtained by subtracting the electronic contribution $\kappa_e = LT/\rho$ (where L is the Lorenz number and ρ is the electrical resistivity) from the total thermal conductivity. As a first approximation, the

temperature dependence of L between 5 and 300 K has been calculated by a single-parabolic band model with acoustic phonon scattering.

^{119}Sn Mössbauer spectra were measured at 5 K in transmission geometry and constant-acceleration mode. The isomer shifts (IS) are referred to $BaSnO_3$ at 300 K. The spectra were fitted by a least-squares method assuming Lorentzian peak shapes. Further analyses of these spectra were realized by a sharpening procedure to simulate the peaks with a linewidth corresponding to the natural emission line.[17] This procedure enables better disentangling overlapping contributions from Sn atoms located on distinct crystallographic sites.

B. Lattice dynamics calculations

Elastic properties calculations were performed by using density function theory (DFT) as implemented in the CASTEP code.[18] During the geometry optimizations, a convergence threshold of 0.02 eV $Å^{-1}$ was used for the residual forces with 0.1 kbar for the pressure. The calculations were performed using a set of norm-conserving pseudopotentials with the PBEsol exchange-correlation functional.[19] The cutoff energy for plane-waves was set to 600 eV. A 16×16×16 k-point mesh was used to sample the Brillouin zone.

C. Inelastic neutron scattering experiments

INS experiments (Ref. 20) were performed at the cold neutron time-of-flight spectrometer IN6-SHARP, operated by the Laboratoire Léon Brillouin (LLB), at the Institut Laue Langevin (Grenoble, France). All measurements were carried out in cryostats under helium atmosphere with an incident neutron wavelength of 4.14 Å.

The powdered samples, of about 15g each, were placed in a niobium cylinder can and measured at $T \approx 100$, 300 and 500 K. The data collected were corrected for empty sample holder scattering, for absorption, for frame overlap and self-attenuation and for different detector efficiencies of the multidetector bank.[20] Because of the difference in scattering powers between the Cu, Sn, V and S atoms (0.126, 0.0412, 0.100 and 0.0320 barns/amu for Cu, Sn, V and S atoms, respectively),[21] the present INS measurements are more sensitive to the Cu and V atoms.

The dynamic structure factors $S(Q, \omega)$ were calculated as an average signal over the scattering angle. The generalized vibrational density of states $G(\omega)$ was derived within the incoherent approximation formalism.[22-25] All the spectra were normalized so that the integral of $G(\omega)$ is equal to the total number of phonon modes, that is, 198 modes for both samples. The positions of the peaks observed in $G(\omega)$ were approximated by Gaussian least-squares fits. For the inelastic signal, only the anti-Stokes line was analyzed due to the limited energy range accessed by IN6 at the Stokes line.

III. Results

A. Mössbauer spectroscopy

Figure 2 presents the Mössbauer spectra collected at 5 K on the L and H samples. Both spectra show a single peak centered near 1.6 mm s^{-1}. The spectrum measured for the H sample is qualitatively similar to those collected on the Zn-substituted colusites $Cu_{26-x}Zn_xV_2Sn_6S_{32}$.[10] In this series, the refinements, performed considering a single doublet centered at 1.53(3) mm s^{-1} with a refined quadrupole splitting (QS) of 0.43(5) mm s^{-1}, are consistent with the presence of only Sn atoms with a +IV oxidation state located in a slightly distorted environment. The

comparison of the two spectra, shown in Figure 2, reveals that the peak for the H sample is significantly broader than that of the L sample, strongly suggesting the presence of higher structural disordering and possibly more than one contribution to the signal. In order to further explore this latter possibility, both spectra have been treated with the sharpening procedure yielding Mössbauer spectra of higher resolutions (lower panels of Figure 2). The sharpened spectrum of the H sample allows to confirm the presence of at least two contributions suggesting the presence of Sn atoms on more than one crystallographic site. Interestingly, for the L sample, the sharpened spectrum evidences shoulders on either side of the main peak, also suggesting the presence of an additional contribution. Assuming two contributions, their respective area fractions strongly depend on the synthesis conditions used, with the amplitude of the second contribution being significantly higher in the H sample than in the L sample. Indeed, the measured Mössbauer spectra can be least-square fitted by considering a singlet and a doublet yielding respective area fractions of 82% and 18% for the L sample, and 35% and 65% for the H sample. The isomer shift of ~ 1.5 mm s^{-1}, refined for both the singlet and the doublet, is consistent with typical values obtained for a +IV oxidation state of Sn atoms. The refined QS of ~ 1.0 mm s^{-1} of the doublet indicates the presence of Sn atoms on another site of the crystal structure exhibiting a slightly distorted environment. Hence, these results indicate that in the L sample, a large majority of Sn atoms (82%) are located on high symmetry site, which is consistent with its expected localization on the 6*c* crystallographic site of local symmetry $\bar{4}$, with the remaining atoms (18%) being in a slightly distorted environment. Of note, because the 6*d* crystallographic site, where Cu atoms reside, is also characterized by a local symmetry $\bar{4}$, a possible localization of Sn atoms on this site cannot be distinguished by Mössbauer spectroscopy. In contrast, in the H sample, only 35% of Sn atoms are located on high symmetry site (*i.e.* 6*c* or 6*d* with the 6*d* site in principle solely occupied by Cu atoms) with the majority of Sn atoms (65%) being on site(s) of lower symmetry (*i.e.* 8*e*

and/or 12*f* sites occupied by Cu atoms of local symmetry 3 or 2, respectively, or interstitial site). These results confirm the +IV oxidation state of Sn atoms in colusite and show that these atoms are not solely located on the 6*c* site but are distributed over at least two distinct crystallographic sites in both samples supporting the presence of antisite defects. Thus, increasing the sintering temperature dramatically alters the distribution of Sn atoms in the crystal structure.

B. Lattice thermal conductivity and specific heat

The main and most remarkable consequence of the higher degree of disorder achieved in the H sample is the significant difference in the temperature dependence of the lattice thermal conductivity κ_L shown in Figure 3. In addition to a strong decrease in the κ_L values, the low-temperature maximum observed for the L sample disappears leaving a temperature dependence that mirrors that of glassy systems. Upon cooling, none of the samples experience a phase transition in contrast to their cousin sulfides tetrahedrites, of general chemical formula $Cu_{12}Sb_4S_{13}$, where structural distortions or exsolution process (*i.e.* a phase separation into two isostructural phases of distinct chemical compositions) have been evidenced below 300 K.[26-31]

Further thermodynamic evidence of the role of the disorder on the thermal transport is provided by the specific heat measurements shown in Figure 4. The low-temperature data are well described up to about 5 K by the conventional Fermi-liquid relation $C_p/T = \gamma + \beta T^2$ where γ is the Sommerfeld coefficient and βT^2 is the phonon contribution with β being related to the Debye temperature $\theta_D = (12\pi^4 RN/5\beta)^{1/3}$. In this relation, R is the gas constant and N is the number of atoms per formula unit. While both samples exhibit similar large γ values of around 55 mJ mol^{-1} K^{-2}, θ_D decreases from 280 K in the L sample to 235 K in the H sample. These values are consistent with those derived for the Zn-substituted colusite

$Cu_{23}Zn_3V_2Sn_6S_{32}$ (Ref. 32) and with those inferred from the measured sound velocities.[13] Furthermore, the lower θ_D value of the H sample compared to the L sample is coherent with the lower sound velocities measured in this sample (4260 m s^{-1} and 2120 m s^{-1} for the longitudinal and transverse sound velocities, respectively, for the L sample compared to 3620 m s^{-1} and 1830 m s^{-1} for the longitudinal and transverse sound velocities, respectively, for the H sample) indicating defect-induced modifications around the acoustic region of the vibrational spectrum.

After subtracting the electronic contribution, the lattice specific heat C_{ph}, plotted as C_{ph}/T^3 versus T to more clearly emphasize the low-energy features, show the presence of specific heat in excess of the Debye contribution for both compounds that peaks near $T_{peak} =$ 15 and 17 K for the H and L samples, respectively. Such an excess has also been observed in tetrahedrites and is often found in cage-like systems for which the low-energy dynamics of the entrapped atoms dominates C_{ph} at low temperatures.[33-42] The amplitude of the peak and the temperature at which it occurs are, however, not strictly equivalent in both compounds with a higher amplitude reached at a lower temperature for the H sample. The temperature of the peak can be related to the characteristic temperature θ_E of low-energy optical modes in the GVDOS usually modelled by Einstein-like contributions. A rough estimate of θ_E can be obtained using the empirical relation suggested to hold in skutterudites and clathrates $\theta_E \approx 5T_{peak}$,[43] yielding $\theta_E \approx$ 75 and 80 K that correspond to features in the GVDOS at ≈ 6.5 and 6.9 meV for the H and L samples, respectively. Both peaks show similar width suggesting that the modes contributing to this excess have similar distribution of energies despite the higher disorder level characterizing the H sample. This finding is coherent with the well-crystallized character of both compounds.

C. Generalized phonon density of states

A comparison of the generalized vibrational density of states $G(\omega)$ measured at 300 K for the L and H samples is shown in Figure 5a. The corresponding Debye plot $G(\omega)/\omega^2$ to stress the low-energy region is presented in Figure 5b. The inelastic signal of the L sample is characterized by three main blocks of modes that extend between 5 and 12 meV, 12 and 22 meV and beyond 30 meV up to the energy cutoff of around 40 meV. The overall shape of $G(\omega)$ is consistent with calculations of the phonon density of states (PDOS) indicating the presence of low-lying optic modes near 7 meV.[13] The lowest peak near 7 meV mainly originates from Cu(12*f*)-weighed modes that dominates the low-energy part of the PDOS. Between 7 and 12 meV, the broad peak observed in $G(\omega)$ mostly results from the contribution of the Cu(6*d*) atoms in addition to lower, but nearly equivalent contributions from the Cu(8*e*), Cu(12*f*), S(8*e*) and Sn(6*c*) atoms. Above 30 meV, the PDOS is mainly dominated by the contribution of the S1 atoms with small admixture of the other elements. While the inelastic spectrum of the H sample shows an overall similar profile, the higher disorder level has two main consequences. First, the entire spectrum, and more specifically the first block near 8 meV, is shifted towards lower energies. Second, the above-mentioned main features are smeared out with a concomitant decrease in their intensity.

The temperature dependence of $G(\omega)$, shown in Figures 6a to 6d for both compounds, does not evidence any significant temperature effect upon warming beyond a mere shift of the entire spectrum indicative of quasi-harmonic behavior. The agreement with a quasi-harmonic approximation is further supported by the comparison of the measured temperature dependence of the lowest peak near 7 meV with that predicted by a quasi-harmonic model of phonon softening. Within this approximation, the temperature dependence of both the phonon frequencies and interatomic force constants is determined through the change in the unit cell

volume due to the thermal expansion. The dependence on volume V of the average phonon energy $\langle E \rangle$ is captured by the average Grüneisen parameter $\overline{\gamma_G}$ via the relation[44]

$$\overline{\gamma_G} = -\frac{\partial ln\langle E \rangle}{\partial lnV} \quad (1)$$

which can be equivalently rewritten as

$$\frac{\Delta E}{E_0} = -\overline{\gamma_G}\frac{\Delta V}{V_0} \quad (2)$$

$\overline{\gamma_G}$ can be expressed in terms of thermodynamic quantities by the relation

$$\overline{\gamma_G} = \frac{\alpha V_m B_S}{C_p} \quad (3)$$

where α is the linear thermal expansion coefficient, V_m is the molar volume, B_S is the isentropic bulk modulus and C_p is the specific heat at constant pressure. $\overline{\gamma_G}$ has been estimated at 300 K using the measured C_p value, an estimate of B_S obtained from the longitudinal and transverse sound velocities measured by a pulse-echo method and α determined from the temperature dependence of the lattice parameter measured by powder X-ray diffraction. Except from α which was found to be nearly identical in both samples with a value of 17.5×10^{-6} K^{-1}, these parameters are not strictly equivalent with respective values of 1174 and 1234 cm^3 mol^{-1}, 152 and 104 GPa and 1592 and 1548 J mol^{-1} K^{-1} for V_m, B_S and C_p for the L and H samples, respectively. Using these values yields thermodynamic average Grüneisen parameters of $\overline{\gamma_G} \approx 1.96$ and 1.45 for the L and H sample, respectively. As shown in Figure

7, the quasi-harmonic prediction, shown as solid lines, agrees well with the temperature dependence observed experimentally. This conventional temperature dependence contrasts with those observed in tetrahedrites, pyrochlores or in the Einstein solids MV$_2$Al$_{20}$ (M = Sc, Al, Ga) where the lowest-energy optical modes significantly shift towards higher energies upon heating, indicative of a high degree of anharmonicity that gives rise to very low lattice thermal conductivity.[20,33,36,37]

Despite the absence of low-energy, strongly anharmonic optical mode, the high values of $\overline{\gamma_G}$ calculated for both samples indicate that some bonding anharmonicity exists in these compounds. These values are consistent with the average Grüneisen parameter of the acoustic modes of 2.18 calculated by density functional theory elastic properties calculations (Table 1) and with the average $\overline{\gamma_{ac}}$ value of 2.05 calculated for the acoustic modes from the phonon calculations shown in a previous study.[13] Furthermore, these values are similar to those observed in AgSbTe$_2$ ($\overline{\gamma_G} \approx 2.05$),[45] Cu$_2$GeSe$_3$ ($\overline{\gamma_G} \approx 1.7$),[46] AgBi$_3S_5$ ($\overline{\gamma_{ac}} \approx 3.6$, averaged only over the acoustic dispersions along the *a*, *b* and *c* crystallographic axes of the crystal structure; Ref. 47) or CsAg$_5$Te$_3$ ($\overline{\gamma_{ac}} \approx 4.2$, averaged only over the acoustic dispersions along the *a*, *b* and *c* crystallographic axes of the crystal structure; Ref. 48), which all exhibit very low lattice thermal conductivity. Because the Umklapp phonon scattering rate scales as γ_G^2, large values are indicative of strong phonon-phonon scattering that helps achieving low κ_L values. More intriguing is the fact that the H sample shows a lower $\overline{\gamma_G}$ value of 1.45 with respect to the L sample despite exhibiting significantly lower κ_L values. The fact that the estimation of $\overline{\gamma_G}$ does not capture the contrast between both samples might indicate that enhanced anharmonicity is not the main driving force in lowering κ_L, suggesting that the high degree of disorder achieved in the H sample is the key property.

IV. Discussion

One of the most important aspects revealed by Mössbauer analysis is the presence of disorder in the L sample, the crystal structure of which had been previously considered as fully-ordered.[10] While the Mössbauer spectra clearly indicate the presence of Sn atoms on other sites of the crystal structure regardless of the synthesis conditions, their exact distribution within the unit cell is however difficult to firmly establish. Based on energy defect calculations, it seems nevertheless clear that antisite defects involving Cu, Sn and V atoms are the main type of defects with indications that Cu_{Sn}, Cu_{Sn} and V_{Cu} on the 6*d*, 8*e* and 12*f*, respectively, have the lowest formation energies (19, 21 and 25 meV, respectively).[13] The possible scenarios regarding the degree of mixed occupancy on these sites is severely constrained by the PXRD data. The fact that the relative intensities of the observed reflections at low angles hardly evolve upon increasing the degree of disorder suggests that the fraction of mixed occupancies should be low enough to leave unchanged these relative intensities but sufficiently high to induce sizeable effects on the lattice parameter and transport properties. We note that the possibility of the presence of two intertwined phases, disordered and ordered, on a macroscopic scale, as evoked for the series of colusites $Cu_{26-x}Nb_2Sn_{6+x}S_{32-x}$ (x = - 0.3, 0, 0.6 and 1.2) for x = 1.2, can be ruled out in the present case.[49] Additional high-resolution synchrotron powder diffraction collected on our samples have not provided any signatures of peak splitting within the experimental resolution of these measurements (not shown). However, these data show that the H sample exhibits broader diffraction peaks compared to the L sample, which supports the higher structural disorder in the former. Further attempts at simulating the PXRD patterns considering various models of Cu, Sn and V distribution did not provide unambiguous information on their positions within the unit cell. For instance, placing Sn atoms on the Cu 8*e* site yields an equivalent structure model demonstrating that the presence of mixed occupancies on these two sites cannot be

distinguished by diffraction data. Moreover, the presence of a well-defined quadrupole splitting indicate that Sn atoms reside in a slightly-distorted tetrahedral environment. However, this distortion is not evidenced by X-ray diffraction which only provides an average view of the atomic environments. Further diffraction experiments probing local environments will be necessary to get more insights into the distribution of these atoms in the H sample.

Increasing the degree of disorder dramatically influences the thermal properties of the samples which acquire several traits that bring them closer to glassy systems, that is, very low lattice thermal conductivity with no Umklapp peak and a smearing out of the GVDOS features. While these two properties are direct consequences of enhanced disorder, the slight but noticeable increase in the low-temperature excess specific heat as well as its shift to lower temperatures may be attributed to the lower density of the sample (4.66 and 4.54 g cm^{-3} for the L and H sample, respectively) rather than reflecting the disorder itself. Recent inelastic X-ray scattering measurements of the PDOS of glasses and their crystalline counterpart have indeed revealed that similar densities of states at low energies and hence, similar excess specific heats emerge when they exhibit similar densities.[50]

Finally, the INS data reveal that the overall temperature evolution of the PDOS can be well described by the quasi-harmonic approximation. The glass-like temperature dependence of κ_L observed in the H sample is thus solely driven by disorder. The lattice distortions induced by the mixed occupation of Cu, Sn and V, and possibly by Cu interstitials, likely strongly lower the acoustic phonon lifetimes via a broadening of the energy width of the acoustic excitations. The similarities between these colusites and the $Ba_{1-x}La_xF_{2+x}$ system,[4,5] where a strong influence of disorder on the thermal transport has also been evidenced, raises interesting questions as to whether the characteristics of the disorder in the latter also applies to colusites. In particular, neutron diffuse scattering on single crystals have revealed that

defects tend to cluster leading to short range ordering,[5] a possibility suggested in these colusites by transmission electron miscroscopy.[13]

IV. Summary and conclusion

In summary, we employed a combination of spectroscopic probes and low-temperature transport and thermodynamic property measurements to get deeper insights into the role played by disorder on the thermal transport of a series of colusites prepared under varying high-temperature conditions. As a sensitive probe of the chemical environment of the Sn atoms, Mössbauer spectroscopy revealed that these atoms are not solely distributed on the 6*c* sites of the colusite crystal structure. This finding supports defect calculations predicting that antisite defects involving Sn atoms have the lowest formation energies. Rather than inducing disorder in the unit cell, increasing the sintering temperature modifies the distribution of the Cu/V/Sn atoms and tends to tip the balance toward a higher concentration of antisite defects. This tunable disorder drives the thermal properties of these compounds closer to those observed in amorphous systems. Regardless of the possible presence of additional interstitial atoms or vacancies, the enhanced disorder does not yield anharmonicity beyond that associated with the thermal expansion of the unit cell. INS data further show the noticeable smearing out of the main features of the PDOS upon disordering, conforming to the evolution of the thermal transport toward a glass-like behavior. These findings suggest that the variations in the thermal properties are solely driven by disorder which strongly shortens acoustic phonon lifetimes. In contrast to tetrahedrites where the glass-like lattice thermal conductivity originates from strongly-anharmonic behavior induced by a peculiarity of the crystal structure, colusites provide an interesting counterexample where a similar behavior

emerges from disorder. The fact that the thermal transport can be easily controlled by varying the sintering parameters may be equally applicable in other sulfur-based compounds, thereby offering a promising strategy for optimizing their thermoelectric performances.

Acknowledgements

The authors acknowledge the CRG for the support of this work and the grant of accessing the IN6 spectrometer of the European neutron source facilities at the Institut Laue Langevin (ILL) in Grenoble (France). The authors would like to thank Christelle Bilot and Jero□me Lecourt for technical support and the financial support of the French Agence Nationale de la Recherche (ANR), through the program Energy Challenge for Secure, Clean and Efficient Energy (Challenge 2, 2015, project MASSCOTE, ANR-15-CE05-0027), FEDER and Normandy Region. M.F. and A.R.S. acknowledge collaboration with the AFLOW Consortium (http://www.aflow.org) under the sponsorship of DOD-ONR (Grants N000141310635 and N000141512266). The work at AIST and Kyushu University was supported as part of the International Joint Research Program for Innovative Energy Technology funded by Ministry of Economy, Trade and Industry (METI) of Japan.

References

[1] S. Ghosh in *Advanced Ceramic Processing*, Chap. 5, A. M. A. Mohamed (Ed.), InTech (2015).

[2] H. J. Goldsmid, Thermoelectric Refrigeration (Springer, New York, 1964).

[3] Thermoelectrics and its Energy Harvesting, edited by D. M. Rowe (CRC Press, Boca Raton, FL, 2012).

[4] D. G. Cahill, S. K. Watson and R. O. Pohl, Phys. Rev. B **46**, 6131 (1992).

[5] N. H. Andersen, K. N. Clausen, J. K. Kjems and J. Schoonman, J. Phys. C: Solid State Phys. **19**, 2377 (1986).

[6] P. G. Spry, S. Merlino, S. Wang, X. Zhang and P. R. Buseck, *Am. Mineral.* **79**, 750 (1994).

[7] O. V. Frank-Kamenetskaya, I. V. Rozhdestvenskaya and L. A. Yanulova, *J. Struct. Chem.* **43**, 89 (2002).

[8] K. Suekuni, F. S. Kim, H. Nishiate, M. Ohta, H. I. Tanaka and T. Takabatake, *Appl. Phys. Lett.* **105**, 132107 (2014).

[9] K. Suekuni, F. S. Kim and T. Takabatake, *J. Appl. Phys.* **116**, 063706 (2014).

[10] C. Bourgès, M. Gilmas, P. Lemoine, N. Mordvinova, O. I. Lebedev, E. Hug, V. M. Nassif, B. Malaman, R. Daou and E. Guilmeau, *J. Mater. Chem. C* **4**, 7455 (2016).

[11] Y. Kikuchi, Y. Bouyrie, M. Ohta, K. Suekuni, M. Aihara and T. Takabatake, *J. Mater. Chem. A* **4**, 15207 (2016).

[12] Y. Bouyrie, V. Ohorodniichuk, S. Sassi, P. Masschelein, A. Dauscher, C. Candolfi and B. Lenoir, *J. Electron. Mater.* **46**, 2684 (2017).

[13] C. Bourgès, Y. Bouyrie, A. R. Supka, R. Al Rahal Al Orabi, P. Lemoine, O. I. Lebedev, M. Ohta, K. Suekuni, V. Nassif, V. Hardy, R. Daou, Y. Miyazaki, M. Fornari and E. Guilmeau, *J. Am. Chem. Soc.* **140**, 2186 (2018).

[14] V. Pavan Kumar, A. R. Supka, P. Lemoine, O. I. Lebedev, B. Raveau, K. Suekuni, V. Nassif, R. Al Rahal Al Orabi, M. Fornari and E. Guilmeau, *Adv. Energy Mater.* **9**, 1803249 (2019).

[15] V. Pavan Kumar, G. Guélou, P. Lemoine, B. Raveau, A. Supka, R. Al Rahal Al Orabi, M. Fornari, K. Suekuni and E. Guilmeau, *Angew. Chem. Int. Ed*. 10.1002/anie.201908579 (2019).

[16] Y. Bouyrie, M. Ohta, K. Suekuni, Y. Kikuchi, P. Jood, A. Yamamoto, T. Takabatake, *J. Mater. Chem. C* **5**, 4174 (2017).

[17] G. Le Caër and R. A. Brand, *J. Phys. Condens. Matter* **10**, 10715 (1998).

[18] S. J. Clark, M. D. Segall, C. J. Pickard, P. J. Hasnip, M. I. J. Probert, K. Refson and M. C. Payne, *Z. Krist.* **220**, 567 (2005).

[19] J. P. Perdew, A. Ruzsinszky, G. I. Csonka, O. A. Vydrov, G. E. Scuseria, L. A. Constantin, X. Zhou and K. Burke, *Phys. Rev. Lett.* **100**, 136406 (2008).

[20] E. Guilmeau, R. Al Rahal AL Orabi, C. Candolfi P. Lemoine, A. Menelle and J.-M. Zanotti, *Inelastic neutron scattering study of the lattice dynamics of colusite*, Institut Laue-Langevin (ILL) doi:10.5291/ILL-DATA.CRG-2549 (2018).

[21] M. M. Koza, A. Leithe-Jasper, E. Sischka, W. Schnelle, H. Borrmann, H. Mutka and Y. Grin, *Phys. Chem. Chem. Phys.* **16**, 27119 (2014).

[22] V. F. Sears, *Neutron News* **3**, 26 (1992).

[23] G. Squires in *Introduction to the Theory of Thermal Neutron Scattering*, Dover Publications, Inc., Mineola, New York (1996).

[24] S. Lovesey in *Theory of Neutron Scattering from Condensed Matter*, Oxford Science Publications, Oxford, UK (1984).

[25] M. M. Bredov, B. A. Kotov, N. M. Okuneva, V. S. Oskotskii and A. L. Shakh-Budagov, *Phys. Solid State* **9**, 214 (1967).

[26] V. S. Oskotskii, *Phys. Solid State* **9**, 420 (1967).

[27] H. I. Tanaka, K. Suekuni, K. Umeo, T. Nagasaki, H. Sato, G. Kutluk, E. Nishibori, H. Kasai and T. Takabatake, *J. Phys. Soc. Jpn.* **85**, 014703 (2016).

[28] D. I. Navasova, V. Yu. Verchenko, A. A. Tsirlin and A. V. Shevelkov, *Chem. Mater.* **28**, 6621 (2016).

[29] F.-H. Sun, C.-F. Wu, Z. Li, Y. Pan, J. Dong and J.-F. Li, *RSC Adv.* **7**, 18909 (2017).

[30] N. Ghassemi, X. Lu, Y. Tian, E. Conant, Y. Yan, X. Zhou and J. H. Ross, *ACS Appl. Mater. Interfaces* **10**, 36010 (2018).

[31] Y. Bouyrie, C. Candolfi, A. Dauscher, B. Malaman and B. Lenoir, *Chem. Mater.* **27**, 8354 (2015).

[32] Y. Yan, H. Wu, G. Wang, X. Lu and X. Zhou, *Energy Storage Mater.* **13**, 127 (2018).

[33] K. Suekuni, H. I. Tanaka, F. S. Kim, K. Umeo and T. Takabatake, *J. Phys. Soc. Jpn.* **84**, 103601 (2015).

[34] Y. Bouyrie, C. Candolfi, S. Pailhès, M. M. Koza, B. Malaman, A. Dauscher, J. Tobola, O. Boisron, L. Saviot and B. Lenoir, *Phys. Chem. Chem. Phys.* **17**, 19751 (2015).

[35] A. F. May, O. Delaire, J. L. Niedziela, E. Lara-Curzio, M. A. Susner, D. L. Abernathy, M. Kirkham and M. A. McGuire, *Phys. Rev. B* **93**, 064104 (2016).

[36] K. Suekuni, C. H. Lee, H. I. Tanaka, E. Nishibori, A. Nakamura, H. Kasai, H. Mori, H. Usui, M. Ochi, T. Hasegawa, M. Nakamura, S. Ohira-Kawamura, T. Kikuchi, K. Kaneko, H.

Nishiate, K. Hashikuni, Y. Kosaka, K. Kuroki and T. Takabatake, *Adv. Mater.* **30**, 1706230 (2018).

[37] H. Mutka, M. M. Koza, M. R. Johnson, Z. Hiroi, J.-I. Yamaura and Y. Nagao, *Phys. Rev. B* **78**, 104307 (2008).

[38] M. M. Koza, H. Mutka, Y. Okamoto, J.-I. Yamaura and Z. Hiroi, *Phys. Chem. Chem. Phys.* **17**, 24837 (2015).

[39] M. A. Avila, K. Suekuni, K. Umeo, H. Fukuoka, S. Yamanaka and T. Takabatake, Phys. Rev. B **74**, 125109 (2006).

[40] C. Candolfi, U. Aydemir, M. M. Koza, M. Baitinger, Yu. Grin and F. Steglich, *J. Phys.: Condens. Matter* **27**, 485401 (2015).

[41] M. M. Koza, L. Capogna, A. Leithe-Jasper, H. Rosner, W. Schnelle, H. Mutka, M. R. Johnson, C. Ritter and Yu. Grin, *Phys. Rev. B* **81**, 174302 (2010).

[42] M. M. Koza, A. Leithe-Jasper, H. Rosner, W. Schnelle, H. Mutka, M. R. Johnson, M. Krisch, L. Capogna and Yu. Grin, *Phys. Rev. B* **84**, 014306 (2011).

[43] K. Matsuhira, C. Sekine, M. Wakeshima, Y. Hinatsu, T. Namiki, K. Takeda, I. Shirotani, H. Sugawara, D. Kikuchi and H. Sato, *J. Phys. Soc. Jpn* **78**, 124601 (2009).

[44] G. Grimvall in *Thermophysical Properties of Materials* (North Holland, Amsterdam, 1999).

[45] D. T. Morelli, V. Jovovic, and J. P. Heremans, *Phys. Rev. Lett.* **101**, 035901 (2008).

[46] J. Y. Cho, X. Shi, J. R. Salvador, G. P. Meissner, J. Yang, H. Wang, A. A. Wereszczak, X. Zhou and C. Uher, *Phys. Rev. B* **84**, 085207 (2011).

[47] G. Tan, S. Hao, J. Zhao, C. Wolverton and M. G. Kanatzidis, *J. Am. Chem. Soc.* **139**, 6467 (2017).

[48] H. Lin, G. Tan, J.-N. Shen, S. Hao, L.-M. Wu, N. Calta, C. Malliakas, S. Wang, C. Uher, C. Wolverton and M. G. Kanatzidis, *Angew. Chem. Int. Ed.* **55**, 1 (2016).

[49] K. Suekuni, Y. Shimizu, E. Nishibori, H. Kasai, H. Saito, D. Yoshimoto, K. Hashikuni, Y. Bouyrie, R. Chetty, M. Ohta, E. Guilmeau, T. Takabatake, K. Watanabe and M. Ohtaki, *J. Mater. Chem. A* **7**, 228 (2019).

[50] A. I. Chumakov, G. Monaco, A. Fontana, A. Bosak, R. P. Hermann, D. Bessas, B. Wehinger,

W. A. Crichton, M. Krisch, R. Ru□ffer, G. Baldi, G. Carini Jr., G. Carini, G. D'Angelo, E. Gilioli,

G. Tripodo, M. Zanatta, B. Winkler, V. Milman, K. Refson, M. T. Dove, N. Dubrovinskaia, L. Dubrovinsky, R. Keding and Y. Z. Yue, *Phys. Rev. Lett.* **112**, 025502 (2014).

Tables

Table 1. Calculated longitudinal (v_l), transverse (v_t), and average (v_m) sound velocities, Poisson ratio (v_p), Young's modulus (E), Grüneisen parameter (γ) and Debye temperature (θ_D) for the colusite $Cu_{26}V_2Sn_6S_{32}$. The bulk modulus and shear modulus are 82 and 26 GPa, respectively.

	v_l $(m\ s^{-1})$	v_t $(m\ s^{-1})$	v_m $(m\ s^{-1})$	v_p	E (GPa)	γ	θ_D (K)
$Cu_{26}V_2Sn_6S_{32}$	4867	2436	2592	0.36	71	2.18	293

Figure Captions

Figure 1. Rietveld refinements of the PXRD data collected at 300 K of the L and H samples. All the reflections can be indexed to the cubic crystal structure of colusites described in the $P\bar{4}3n$ space group. Inset: Perspective view of the crystal structure of the colusite $Cu_{26}V_2Sn_6S_{32}$. The Cu atoms on the 8*e*, 6*d* and 12*f* sites are shown in dark green, light green and light blue, respectively. The Sn atoms on the 6*c* site are in dark blue while the S atoms on the 8*e* and 24*i* sites are shown in yellow and brown, respectively. The V atoms on the 2*a* site are shown in red.

Figure 2. (Upper panels) ^{119}Sn Mössbauer spectra collected at T = 4.2 K of the L and H samples sintered at 873 and 1023 K, respectively. (Lower panels) Spectra obtained by the thinning procedure highlighting the presence of the two contributions to the Mössbauer signal in both samples.

Figure 3. Temperature dependence of the lattice thermal conductivity κ_L of the L and H samples.

Figure 4. Lattice contribution to the specific heat C_{ph} plotted as C_{ph}/T^3 versus temperature on a logarithmic scale for the L and H samples.

Figure 5. (a) Generalized vibrational density of states $G(\omega)$ of the L and H samples determined from INS measurements at 300 K. For both compounds, the spectra were normalized so that the integral of $G(\omega)$ corresponds to 198 phonon modes. (b) Debye plots $G(\omega)/\omega^2$ for both samples that stress the low-energy region of the $G(\omega)$ spectra. The color-coded symbols are similar in both panels.

Figure 6. Temperature dependence of the generalized vibrational density of states $G(\omega)$ of the a) L and b) H samples. The corresponding Debye plots $G(\omega)/\omega^2$ are shown in panels c) and d) for the L and H samples, respectively. The temperature- and color-coded symbols are reported in the figures.

Figure 7. Temperature dependence of the characteristic energy (filled circle symbols) of the low-energy peak at 7 meV obtained from fits to the $G(\omega)/\omega^2$ data with Gaussian functions. The solid lines correspond to the quasi-harmonic prediction of the temperature dependence of the low-energy peak using thermodynamic average Grüneisen parameters of 1.96 and 1.45 for the L and H sample, respectively.

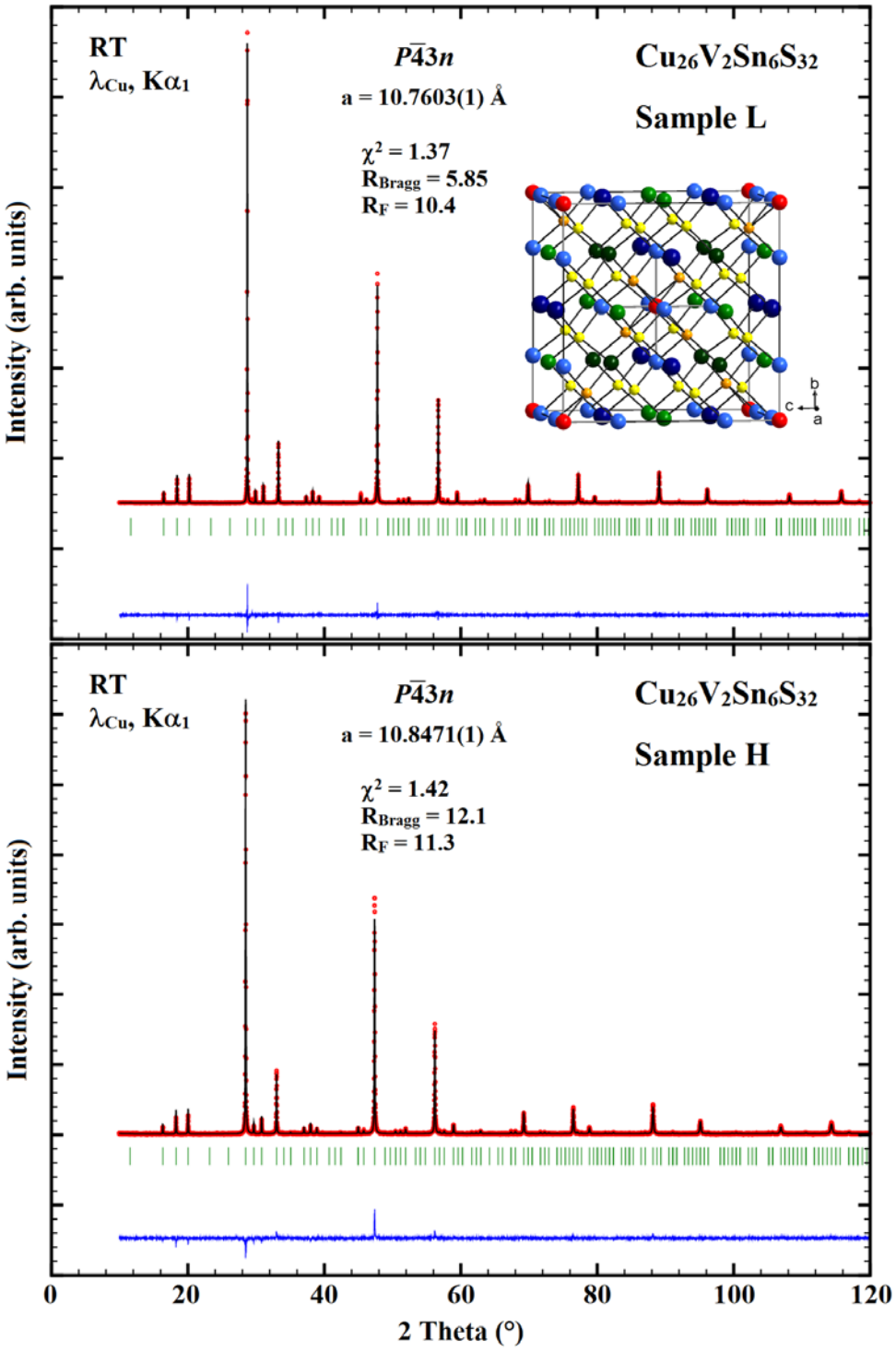
RT
λCu, Kα1
P4̄3n
a = 10.7603(1) Å
χ² = 1.37
RBragg = 5.85
RF = 10.4
Cu26V2Sn6S32
Sample L
b
c
a
Intensity (arb. units)
RT
λCu, Kα1
P4̄3n
a = 10.8471(1) Å
χ² = 1.42
RBragg = 12.1
RF = 11.3
Cu26V2Sn6S32
Sample H
Intensity (arb. units)
0
20
40
60
80
100
120
2 Theta (°)

Figure 1

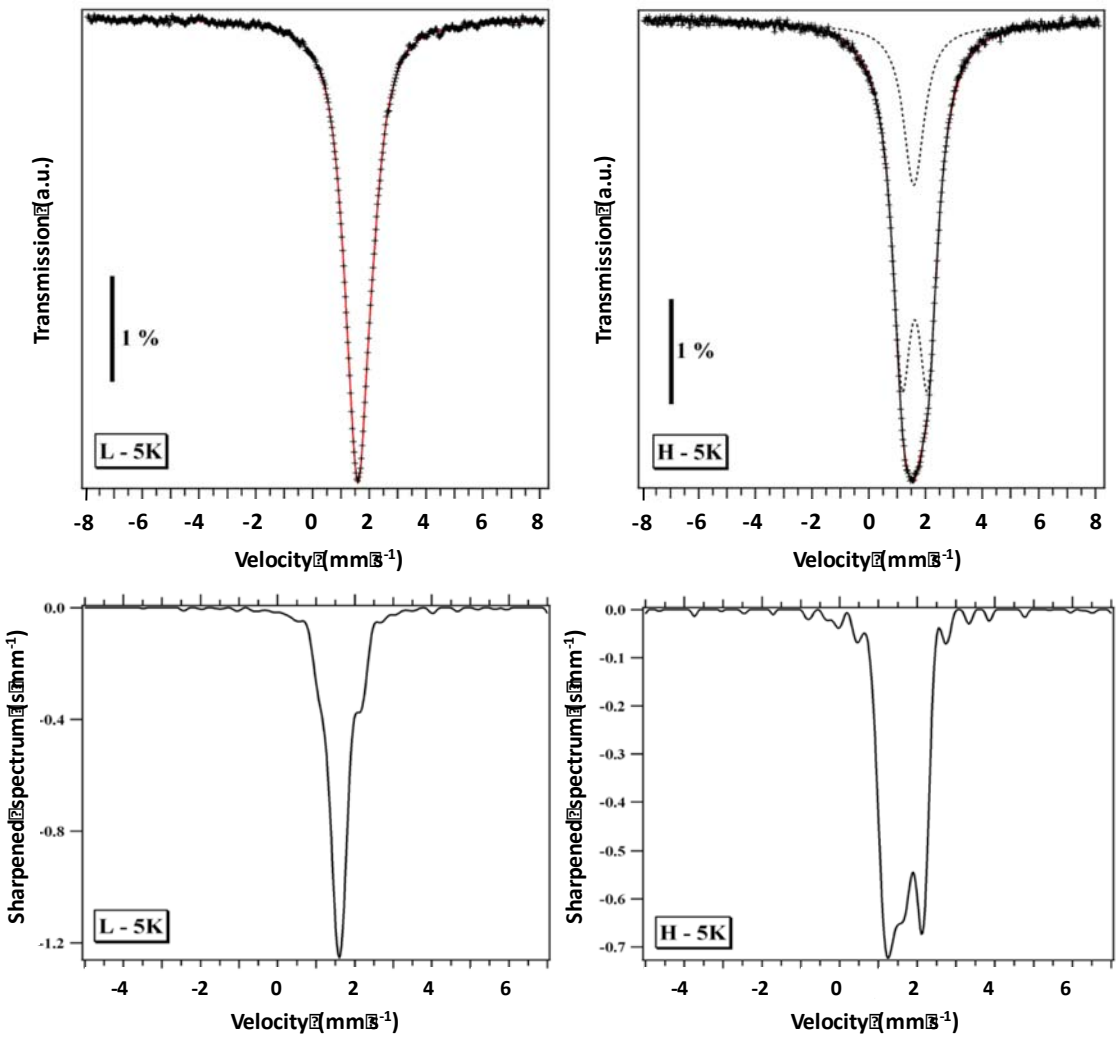
Transmission (a.u.)
1 %
L - 5K
H - 5K
Velocity (mms-1)
Sharpened spectrum (s mm-1)

Figure 2

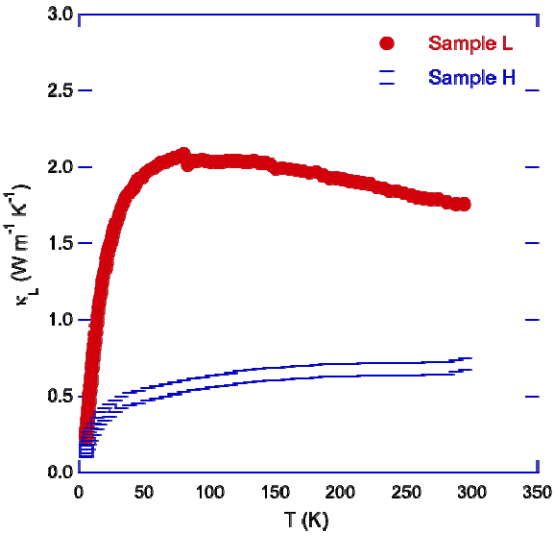
Sample L
Sample H
κ_L (W m^{-1} K^{-1})
T (K)
3.0
2.5
2.0
1.5
1.0
0.5
0.0
0
50
100
150
200
250
300
350

Figure 3

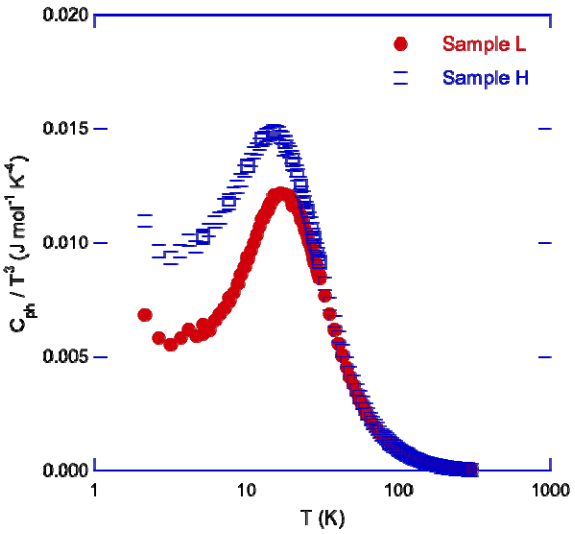
0.020
0.015
0.010
0.005
0.000
1
10
100
1000
T (K)
C_{ph} / T^3 (J mol^{-1} K^{-4})
Sample L
Sample H

Figure 4

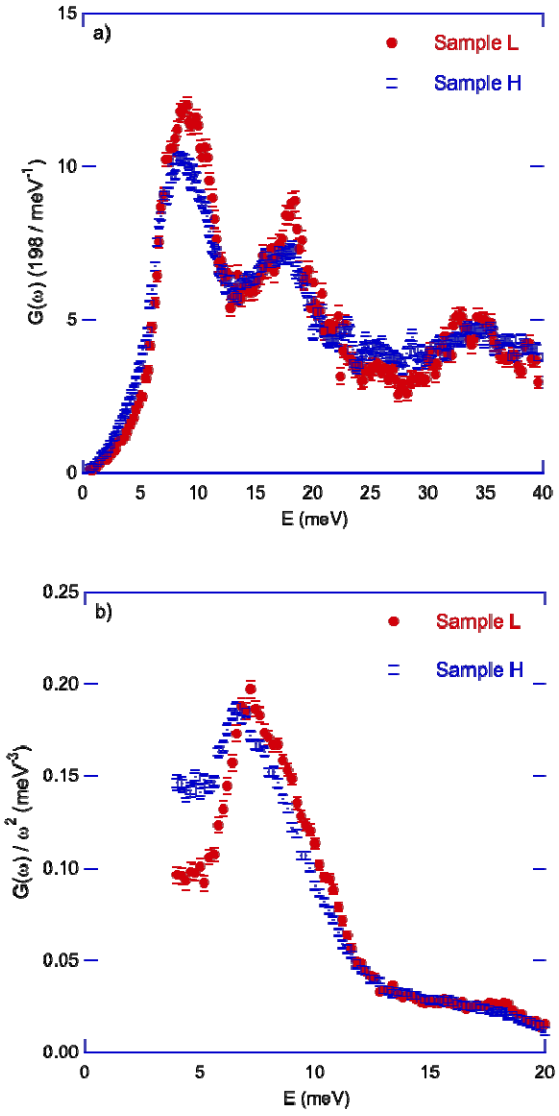
a)
Sample L
Sample H
G(ω) (198 / meV^{-1})
E (meV)
b)
Sample L
Sample H
G(ω) / ω^2 (meV^{-3})
E (meV)

Figure 5

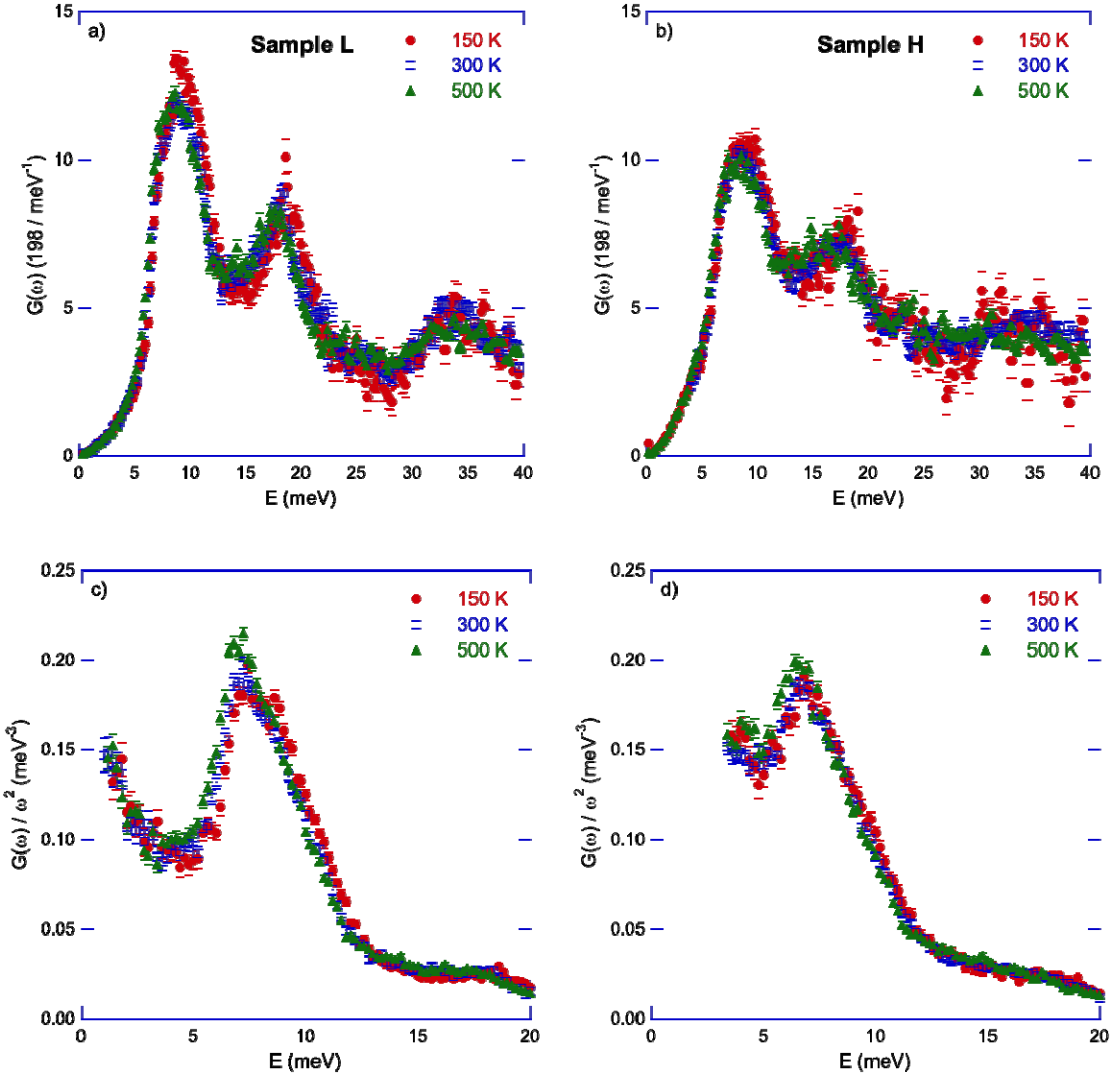
a)
Sample L
150 K
300 K
500 K
G(ω) (198 / meV^{-1})
E (meV)
b)
Sample H
150 K
300 K
500 K
G(ω) (198 / meV^{-1})
E (meV)
c)
150 K
300 K
500 K
G(ω) / ω^2 (meV^{-3})
E (meV)
d)
150 K
300 K
500 K
G(ω) / ω^2 (meV^{-3})
E (meV)

Figure 6

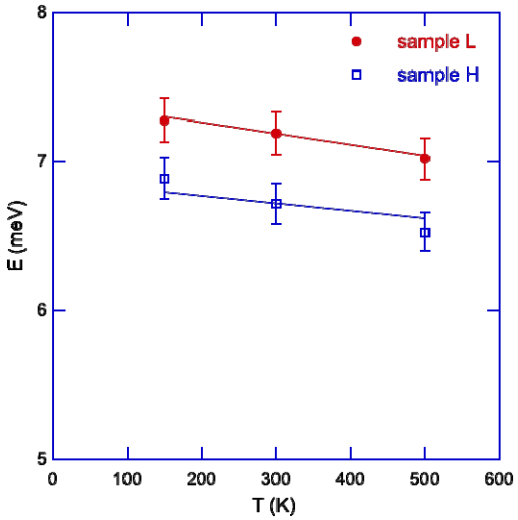

Figure 7